J Nanopart Res (2011) 13:4623–4630
DOI 10.1007/s11051-011-0426-8

RESEARCH PAPER

Antiferromagnetic interactions in Er-doped SnO_2 DMS nanoparticles

S. Sambasivam · D. Paul Joseph · Jung Hyun Jeong · Byung Chun Choi · Kwon Taek Lim · Sang Su Kim · Tae Kwon Song

Received: 4 August 2010 / Accepted: 13 May 2011 / Published online: 26 May 2011

Abstract Diluted magnetic semiconductor (DMS) nanoparticles of $Sn_{1-x}Er_xO_2$ ($x = 0.0$, 0.02, 0.04, and 0.1) were prepared by sol–gel method. The X-ray diffraction patterns showed SnO_2 rutile structure for all samples with no impurity peaks. The decrease in crystallite size with Er concentration was confirmed from TEM measurements (from 12 to 4 nm). The UV–Visible absorption spectra of Er-doped SnO_2 nanoparticles showed blue shift in band gap compared to undoped SnO_2. The electron spin resonance analysis of Er-doped SnO_2 nanoparticles indicate Er^{3+} in a rutile lattice and also decrease in intensity with Er concentration above $x = 0.02$. Temperature-dependent magnetization studies and the inverse susceptibility curves indicated increased antiferromagnetic interaction with Er concentration.

Keywords DMS · Nanoparticles · SnO_2:Er · ESR · Magnetic studies · Electron spin

S. Sambasivam · J. H. Jeong · B. C. Choi (✉)
Department of Physics, Pukyong National University, Busan 608-737, South Korea
e-mail: bcchoi@pknu.ac.kr

D. Paul Joseph
Center for Condensed Matter Sciences, National Taiwan University, Taipei 10617, Taiwan

K. T. Lim
Image System Science & Engineering, Pukyong National University, Busan 608-737, Korea

S. S. Kim
Department of Physics, Changwon National University, Changwon 641-773, Korea

T. K. Song
Department of Ceramic Science and Engineering, Changwon National University, Changwon 641-773, Korea

Introduction

Diluted magnetic semiconductors (DMS) (Ohno 1998) produced by doping transition metal or rare earth metal ions into non-magnetic semiconductors have been of great interest to realize spintronics devices such as spin LED (Fiederling et al. 1999, p 787), spin field effect transistor (Datta and Das 1990), etc., in the near future. Some authors report ferromagnetic behavior at room temperature in pure TiO_2, HfO_2, and ZnO nanoparticles (Coey et al. 2005; Hong et al. 2006; Dietl et al. 2000) due to defects and or oxygen vacancies, hence it is crucial to differentiate the source of magnetism intrinsic either from the dopant or from impurity phases. Lee et al. (2003) reported magnetization of Fe-doped TiO_2 samples to decrease with Fe composition. Apart from oxides, transition metal doped semiconductor systems such as (GaMn)As (Ohno et al. 1996), (GaMn)N (Reed et al. 2001), (InMn)As (Ohno et al. 1992), and Cr-doped

$CuZnSe_2$ (Paul Joseph and Venkateswaran 2010) DMS also exhibit ferromagnetism. Recently, a wide variety of magnetic behavior was observed in SnO_2 doped with V, Cr, Mn, Fe, Co, and Ni (Hong and Sakai 2005; Fitzgerald et al. 2004; Wang et al. 2006; Hong et al. 2005; Ogale et al. 2003; Coey et al. 2004).

Tin dioxide is an n-type wide band gap semiconductor that has variety of applications such as solid-state gas sensors, surge arresters, transparent conductors and oxidation catalysts (Fukano et al. 2005; Paul Joseph et al. 2009; Korotcenkov 2005). 'Er' has been doped into SnO_2 and studied mainly for its optical properties (Brovelli et al. 2006; Wu and Coffer 2007; Morais and Luis Scalvi 2007) and a very few from DMS point of view (Mohan Kant et al. 2005). SnO_2-based powders are obtained by means of a variety of synthesis techniques including the mixed oxides route, co-precipitation and sol–gel methods (Wang et al. 1994; Tarey and Raju 1985; Minami et al. 1988). In this study, we prepared Er^{3+}doped SnO_2 nanoparticles by sol–gel technique, a method employed quite frequently to synthesize nanoparticles because of its low cost and good stoichiometric control. The structural, optical, morphological, and magnetic properties of the prepared nanoparticles are investigated.

Experimental details

Synthesis of Er-doped SnO_2 nanoparticles

Undoped and Er-doped SnO_2 DMS nanoparticles were prepared by a sol–gel technique. To achieve the required composition of $Sn_{1-x}Er_xO_2$ ($x = 0.0$, 0.02, 0.04, and 0.1), appropriate amount of tin chloride ($SnCl_4{\cdot}5H_2O$) and erbium chloride ($ErCl_3{\cdot}6H_2O$) was dissolved in 75 mL of distilled water at 80 °C along with 6 mL of polyglycol and citric acid (to attain pH = 1.5) was continually stirred for 10 min until a sol is formed. Ammonia solution ($NH_3{\cdot}H_2O$ (28%)) was added drop wise to the above mixture until pH = 8. The formed hydroxide product was stirred for 3 h to form a gel, and finally dried at 120 °C/12 h and calcined at 400 °C/2 h in air.

Measurements

The X-ray diffraction (XRD) patterns were obtained using X'PERT PRO X-ray diffractometer with $CuK_\alpha = 1.5406$ Å radiation. Transmission Electron Micrographs (TEM) were recorded in (JEOL-TEM 2010) with an accelerating voltage of 200 kV. The optical absorption measurements were performed in a JASCO-V-670 spectrophotometer. Electron spin resonance (ESR) spectra of powder samples were recorded at room temperature using X-Band JEOL, JES PX 2300 spectrometer in the frequency range of 8.8–9.6 GHz. The magnetic measurements were carried out using a superconducting quantum interference device (SQUID, Quantum Design MPMS-XL7).

Results and discussion

The XRD patterns of $Sn_{1-x}Er_xO_2$ (with $x = 0.0$, 0.02, 0.04, and 0.1) DMS nanoparticles (Fig. 1) reveal that all the samples have a rutile-type cassiterite (tetragonal) phase of SnO_2, and the doping does not change the tetragonal structure (JCPDS # 41-1445) of SnO_2. Furthermore, we could not find any diffraction peak corresponding to any impurity phase within the limit of instrumental sensitivity. The peak positions do not show any measurable change, while the intensities of the peaks increase with increasing Er content. The diffraction peaks of undoped SnO_2 are broadened and the average crystallite size was estimated to be 16.1 nm. As Er content increases, the XRD peaks appear to be sharper with decreased full width at half

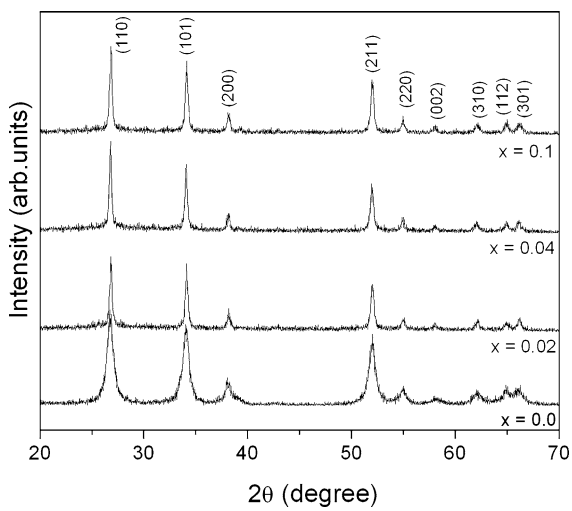

Fig. 1 XRD patterns of $Sn_{1-x}Er_xO_2$ ($x = 0.0$, 0.02, 0.04, and 0.1) nanoparticles

Table 1 Average crystallite size, band gap and g values of $Sn_{1-x}Er_xO_2$ ($x = 0.0$, 0.02, 0.04, and 0.1) nanoparticles

Composition (x)	Average crystallite size from XRD (nm)	Band gap (eV)	g values from ESR
0.0	16.1	3.73	–
0.02	16.8	3.79	2.00148
0.04	17.3	3.81	2.00145
0.1	18.6	3.91	2.00145

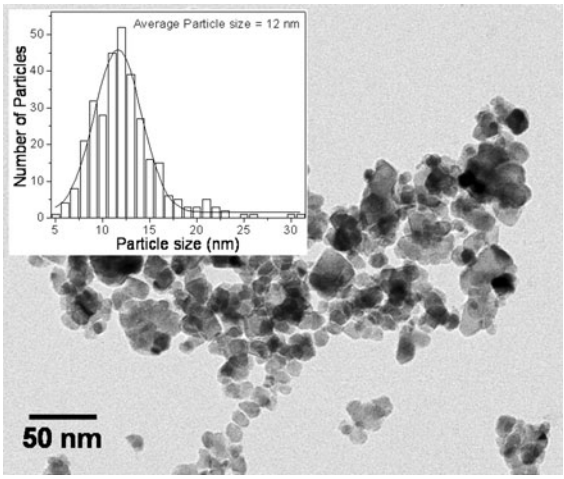

Fig. 2 TEM micrograph of $Sn_{1-x}Er_xO_2$ ($x = 0.02$) nanoparticles with the *inset* showing the size distribution plot

the maximum (FWHM), indicating possible increase in crystallite size. The average crystallite size of the Er-doped samples was found to be in the range 16–19 nm using the Scherrer equation (Table 1). The TEM measurements were performed to confirm the nanocrystalline nature and to study the morphology of the particles. Typical TEM micrograph of $Sn_{1-x}Er_xO_2$ ($x = 0.02$) sample (Fig. 2) shows well isolated and nearly spherical shaped crystallites. The distribution plot fitted with a Gaussian profile (Inset of Fig. 2) shows narrow distribution in size with an average crystallite size of 12 nm. The TEM micrograph and SAED pattern of sample with $x = 0.04$ also show well isolated nanoparticles (Fig. 3). The high resolution TEM image of sample with $x = 0.04$ shows highly crystallized spherical and few elongated particles with clear lattice fringes and with almost no grain boundaries (Fig. 4). The calculated d spacing value of 1.18 Å for the lengthy elongated rod correspond to the (400) plane (JCPDS # 41-1445).

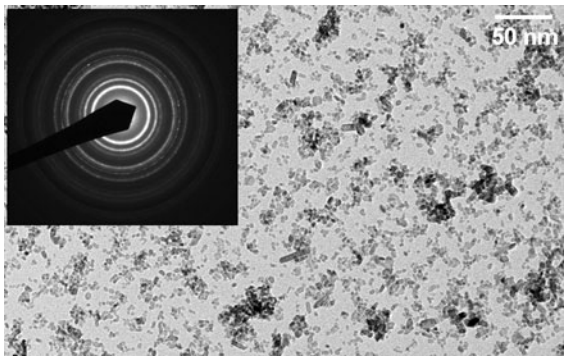

Fig. 3 TEM micrograph of $Sn_{1-x}Er_xO_2$ ($x = 0.04$) sample showing smaller sized nanoparticles. *Inset* is the SAED pattern

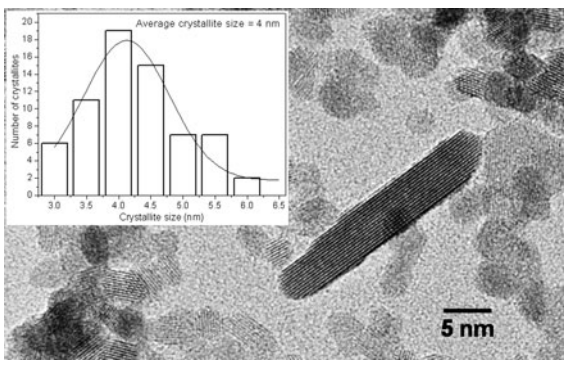

Fig. 4 High resolution TEM micrograph of $Sn_{1-x}Er_xO_2$ ($x = 0.04$) nanoparticles with the *inset* showing the size distribution plot

The elongated rod was found to have high aspect ratio of 5.33. The estimated average crystallite size from size distribution plot (Inset of Fig. 4) is 4 nm. The average crystallite size estimated from XRD and TEM have contradicting trend. In this case, due to the method of preparation and subsequent annealing, the particles are well crystallized and hence the FWHM value decreases indicating increasing crystallite size with Er concentration. However, the direct observation by TEM and analysis of the data confirms decrease in size with Er concentration.

The optical properties of semiconductor nanoparticles exhibiting interesting behavior have been studied extensively in recent years. Optical absorption spectra of $Sn_{1-x}Er_xO_2$ ($x = 0.0$, 0.02, 0.04, and 0.1) nanoparticles shown in Fig. 5 indicate absorption edge to shift to shorter wavelengths implying a blue shift in band gap with respect to bulk SnO_2 (3.6 eV at 300 K). Similar blue shift in band gap has been

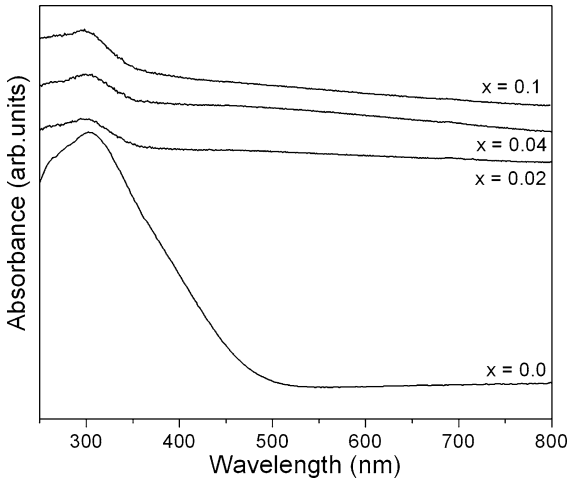

Fig. 5 Optical absorption spectra of $Sn_{1-x}Er_xO_2$ ($x = 0.0$, 0.02, 0.04, and 0.1) nanoparticles

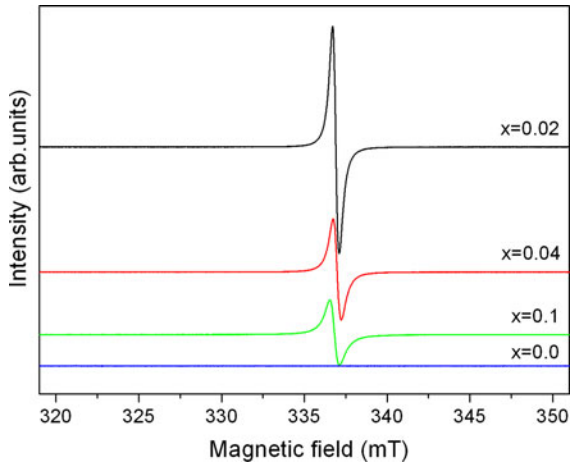

Fig. 6 The ESR spectra of $Sn_{1-x}Er_xO_2$ ($x = 0.0$, 0.02, 0.04, and 0.1) samples

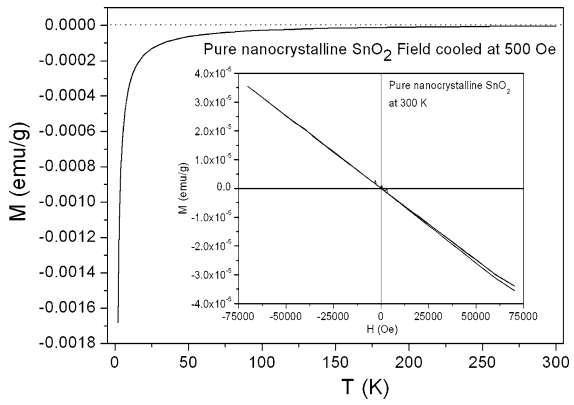

Fig. 7 The diamagnetic behavior of nanocrystalline SnO_2 sample as a function of temperature. *Inset* shows the field dependent diamagnetic signal at 300 K

observed in the case of pure SnO_2 due to size effect by Das et al. (2006). This blue shift in band gap is due to size effect, and observed when the particle size of a semiconductor becomes comparable to the Bohr radius of the exciton leading to variations in the properties of the material due to quantum confinement. The increase in band gap value with decreasing crystallite size induced by Er content is listed in Table 1.

The ESR technique has been employed to study rare earth ions in a variety of host lattices (Abragam and Bleany 1970) in which the study of ground state of the rare earth impurity reveals the symmetry of the occupied state. The ESR spectra of Er^{3+} in SnO_2 have been recorded at room temperature in the field range 320–350 mT, at 100 kHz field modulation to obtain the first derivative spectrum. No resonance signal was detected in the ESR spectra of undoped SnO_2 nanoparticles. Figure 6 shows the single resonance peak observed for $Sn_{1-x}Er_xO_2$ ($x = 0.0$, 0.02, 0.04, and 0.1) samples confirming Er^{3+} ion substituting the Sn^{4+} sites. This resonance signal could be attributed to Er^{3+} ions in SnO_2 nanoparticles due to ground state of free Er^{3+} ion in $4f^{11}$ electronic configuration (Yang et al. 2009). The g values of Er-doped samples are listed in Table 1. Ting et al. (2001) reported g value of 2.0 for a relatively small peak of Er^{3+} doped TiO_2. The intensity of ESR signal is initially high for $x = 0.02$ and then it decreases with increasing Er content which may be because of the possibility of antiferromagnetic interactions induced in the sample due to higher Er concentration.

The temperature dependent (M(T)) (at 500 Oe) and field dependent (M(H)) (at 300 K) magnetization measurement of undoped nanocrystalline SnO_2 sample exhibits diamagnetic nature (Fig. 7) confirming that there is no positive susceptibility contribution from defects and oxygen vacancies of SnO_2 which has been cautioned to be a universal feature of non-magnetic oxide nanoparticles (Sundaresan et al. 2006). The magnetic hysteresis loops measured at 5 and 300 K of $Sn_{1-x}Er_xO_2$ with $x = 0.04$ and 0.1 nanoparticles are shown in Figs. 8 and 9, respectively. The magnetization at 5 K, though very small due to the doped Er^{3+} ions, it is comparatively higher

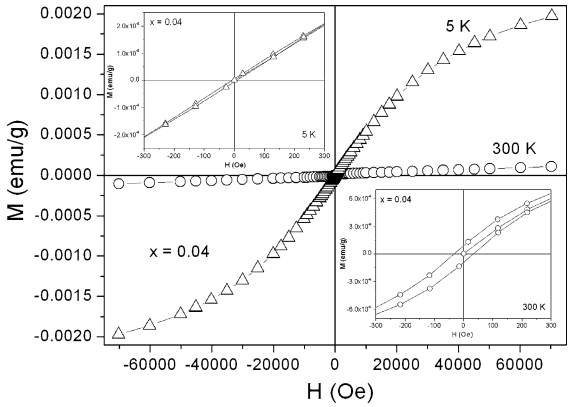

Fig. 8 The M(H) curves of $Sn_{1-x}Er_xO_2$ ($x = 0.04$) nanoparticles at 5 and 300 K. *Insets* show the hysteresis behavior at lower fields

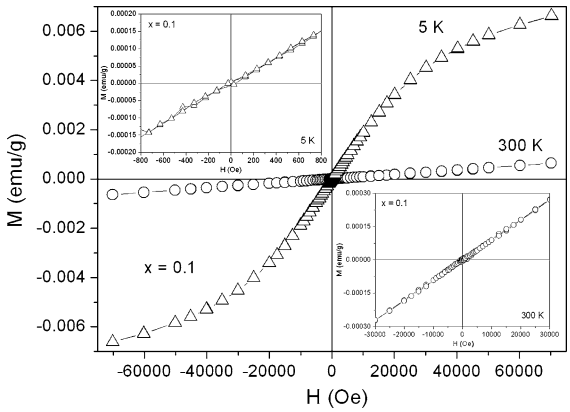

Fig. 9 The M(H) curves of $Sn_{1-x}Er_xO_2$ ($x = 0.1$) nanoparticles at 5 and 300 K. *Insets* show the paramagnetic behavior without any hysteresis behavior at lower fields

than that at 300 K. It can be seen that hysteresis with a small coercivity (34 Oe) is observed at room temperature for $x = 0.04$ (bottom inset of Fig. 8) which is not the case at 5 K (top inset of Fig. 8) indicating loss of the observed weak magnetic behavior at low temperatures. For $x = 0.1$, we do not observe any hysteresis behavior both at 5 and 300 K (Top and bottom inset of Fig. 9) indicating loss of weak ferromagnetic behavior with increasing Er concentration. This behavior can be justified considering antiferromagnetic interactions to increase with Er content thereby decreasing the observed weak ferromagnetic interactions. Mohan Kant et al. (2005) reported intrinsic ferromagnetism in rare earth (Gd,

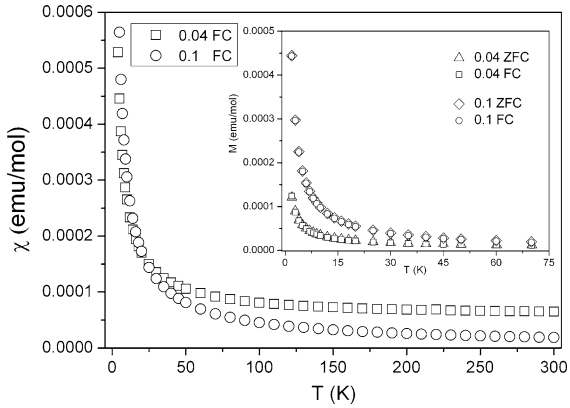

Fig. 10 The molar susceptibility curves calculated from field-cooled (at 500 Oe) curves of $Sn_{1-x}Er_xO_2$ ($x = 0.04$ and 0.1) nanoparticles. The *inset* shows the ZFC–FC behavior of the samples

Dy, and Er) doped SnO_2 thin films by pulsed laser deposition. However, antiferromagnetic behavior has also been reported in the case of Co-doped ZnO and Fe-doped ZnO, TiO_2, and SnO_2 (Bouloudenine et al. 2005; Soumahoro et al. 2010; Lee et al. 2003; Sambasivam et al. 2011). Lawes et al. (2005) reported antiferromagnetic interactions in Mn- and Co-doped ZnO to depend on concentration of the magnetic dopant.

The molar susceptibility ($\chi(T)$) plot from the temperature-dependent magnetization (M(T)) of the $Sn_{1-x}Er_xO_2$ ($x = 0.04$ and 0.1) nanoparticles under field-cooled (FC) (at 500 Oe) mode are shown in Fig. 10. Significant decrease in the positive susceptibility is observed with Er content increasing from 0.04 to 0.1 in the temperature range 300–50 K, below which the susceptibility merge and start increasing. The M(T) curves of $x = 0.04$ and 0.1 show a steep rise in magnetization value below 50 K without any distinct magnetic phase transition. There is no bifurcation observed between the ZFC–FC curves of $x = 0.04$ and 0.1 (Inset of Fig. 10), thereby indicating absence of intrinsic ferromagnetic behavior in the samples.

The $\chi(T)$ of $Sn_{1-x}Er_xO_2$ ($x = 0.04$ and 0.1) (Figs. 11 and 12) are fitted to Curie–Weiss law

$$\chi = \frac{C}{T + \theta} \tag{1}$$

where C is the Curie constant, θ is the Curie–Weiss temperature, and T is the temperature.

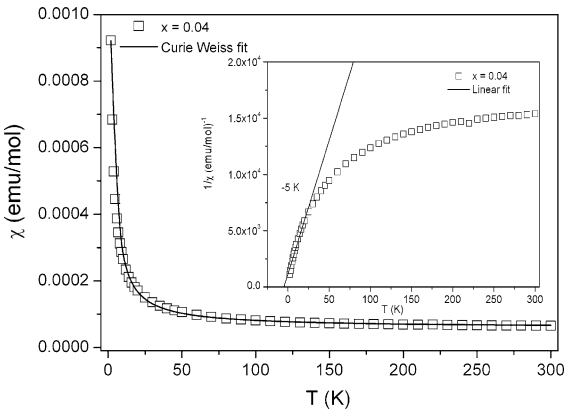

Fig. 11 The molar susceptibility curves calculated from field-cooled (at 500 Oe) curves of $Sn_{1-x}Er_xO_2$ ($x = 0.04$) nanoparticles. The *inset* shows the variation of inverse susceptibility with temperature

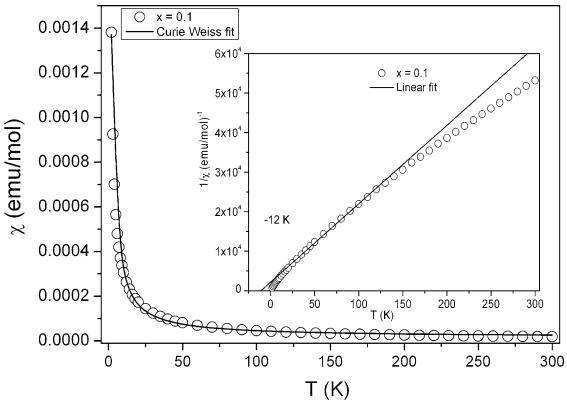

Fig. 12 The molar susceptibility curves calculated from field-cooled (at 500 Oe) curves of $Sn_{1-x}Er_xO_2$ ($x = 0.1$) nanoparticles. The *inset* shows the variation of inverse susceptibility with temperature

The inverse susceptibility ($1/\chi(T)$) of x = 0.04 sample (Inset of Fig. 11) has a nearly flat region starting from 300 to around 175 K, below which there is a distinct curvature up to 5 K. In order to obtain θ, which reflects the strength and nature of the magnetic interaction, we have extrapolated the straight line fitting of the linear region at low temperatures of $1/\chi(T)$. The intercept of the extrapolated line yielded a negative value of −5 K indicating presence of antiferromagnetic interactions. For $x = 0.1$, the behavior of $\chi(T)$ (Fig. 12) is similar to that of $x = 0.04$, however, the $1/\chi(T)$ of $x = 0.1$ (Inset of Fig. 12) is distinctly different with less curvature and more or less similar to a straight line. The linear fit intercept at −12 K indicates increased antiferromagnetic interactions on increasing Er content to $x = 0.1$. The value of θ being negative for Er-doped SnO_2 samples, −5 K for $x = 0.04$ and −12 K for $x = 0.1$ confirms the presence of antiferromagnetic interactions.

According to RKKY theory (Ruderman and Kittel 1954; Yosida 1957), the observed magnetic properties are due to the exchange interaction between local spin-polarized electrons (such as the electrons of Er^{3+} ions) and conduction electrons. The conduction electrons are regarded as a media to interact among the Er^{3+} ions. This interaction leads to the spin polarization of conduction electrons. Subsequently, the spin-polarized conduction electrons perform an exchange interaction with local spin-polarized electrons of other Er^{3+} ions. However, the exchange interaction is short ranged and oscillating nature based on the concentration of Er and its nearest neighbor distance. This may be the plausible explanation of the observed antiferromagnetic interactions.

Conclusion

$Sn_{1-x}Er_xO_2$ ($x = 0.0$, 0.02, 0.04, and 0.1) DMS nanoparticles prepared by sol–gel technique had rutile structure without any impurities as confirmed by XRD and TEM measurements. High resolution TEM results indicate the nanoparticles to be highly crystalline and the crystallite size to decrease with increasing Er content. The optical absorption spectra showed blue shift in band gap with increasing Er content in SnO_2 nanoparticles due to size effect. ESR analysis shows a single resonance peak due to Er in 3+ state in SnO_2 and also decrease in intensity above $x = 0.02$ Er content. The inverse susceptibility data from the field-cooled and zero-field-cooled magnetization measurements reveal that Er-doped SnO_2 nanoparticles tend toward antiferromagnetic behavior with Er content.

Acknowledgments This study was supported by Priority Research Centers Program through the National Research Foundation of Korea (NRF) funded by the Ministry of Education, Science and Technology (2009-0094064), and supported by the Korea Science and Engineering Foundation (KOSEF) grant funded by the Korea government (MEST) (R01-2008-000-21056-0).

References

Abragam A, Bleany B (1970) Electron paramagnetic resonance of transition ions. Clarendon, Oxford

Bouloudenine M, Virat N, Colis S, Kortus J, Dinia A (2005) Antiferromagnetism in bulk $Zn_{1-x}Co_xO$ magnetic semiconductors prepared by the coprecipitation technique. Appl Phys Lett 87:052501. doi:10.1063/1.2001739

Brovelli S, Baraldi A, Capelletti R, Chiodini N, Lauria A, Mazzera M, Monguzzi A, Paleari A (2006) Growth of SnO_2 nanocrystals controlled by erbium doping in silica. Nanotechnology 17:4031–4036. doi:10.1088/0957-4484/17/16/006

Coey JMD, Douvalis AP, Fitzgerald CB, Venkatesan M (2004) Ferromagnetism in Fe-doped SnO_2 thin films. Appl Phys Lett 84:1332–1334. doi:10.1063/1.1650041

Coey JMD, Venkatesan M, Stamenov P, Fitzgerald CB, Dorneles LS (2005) Magnetism in hafnium dioxide. Phys Rev B 72:024450. doi:10.1103/PhysRevB.72.024450

Das S, Kar S, Chaudhuri S (2006) Optical properties of SnO_2 nanoparticles and nanorods synthesized by solvothermal process. J Appl Phys 99:114303(1)–114303(7). doi:10.1063/1.2200449

Datta S, Das B (1990) Electronic analog of the electro-optic modulator. Appl Phys Lett 56:665–667. doi:10.1063/1.102730

Dietl T, Ohno H, Matsukura F, Cibert J, Ferrand D (2000) Zener model description of ferromagnetism in zinc-blende magnetic semiconductors. Science 287:1019–1022. doi:10.1126/science.287.5455.1019

Fiederling R, Kleim M, Reuscher G, Ossau W, Schmidt G, Waag A, Molenkamp LW (1999) Injection and detection of a spin-polarized current in a light emitting diode. Nature 402:787–790. doi:10.1038/45502

Fitzgerald CB, Venkatesan M, Douvalis AP, Huber S, Coey JMD, Bakas T (2004) SnO_2 doped with Mn, Fe or Co:RT DMS. J Appl Phys 95:7390–7392. doi:10.1063/1.1676026

Fukano T, Ida T, Hashizume H (2005) Ionization potentials of transparent conductive indium tin oxide films covered with a single layer of fluorine-doped tin oxide nanoparticles grown by spray pyrolysis deposition. J Appl Phys 97:084314(1)–084314(6). doi:10.1063/1.1866488

Hong NH, Sakai J (2005) Ferromagnetic V-doped SnO_2 thin films. Physica B 358:265–268. doi:10.1016/j.physb.2005.01.456

Hong NH, Sakai J, Prellier W, Hassini A (2005) Transparent Cr-doped SnO2 thin films: ferromagnetism beyond RT with a giant magnetic moment. J Phys 17:1697–1702. doi:10.1088/0953-8984/17/10/023

Hong NH, Sakai J, Poirot N, Brize V (2006) RT ferromagnetism observed in undoped semiconducting and insulating oxide thin films. Phys Rev B 73:132404(1)–132404(4). doi:10.1103/PhysRevB.73.132404

Korotcenkov G (2005) Gas response control through structural and chemical modification of metal oxide films: state of the art and approaches. Sens Actuator B 107:209–232. doi:10.1016/j.snb.2004.10.006

Lawes G, Risbud AS, Ramirez AP, Seshadri R (2005) Absence of ferromagnetism in Co and Mn substituted polycrystalline ZnO. Phys Rev B 71:045201. doi:10.1103/PhysRevB.71.045201

Lee HM, Kim SJ, Shim I-B, Kim CS (2003) Mössbauer studies of 57Fe-doped anatase TiO_2. IEEE Trans Magn 39:2788–2790

Minami T, Nanto H, Takata S (1988) Highly conducting and transparent SnO_2 thin films prepared by RF magnetron sputtering on low temperature substrates. Jpn J Appl Phys 27:L287–L289. doi:10.1143/JJAP.27.L287-L289

Mohan Kant K, Chandrasekaran K, Ogale SB, Venkatesan T, Sethupathi K, Rao MSR (2005) Magnetic and optical properties of rare earth doped $Sn_{0.95}RE_{0.05}O_2$ (RE = Gd, Dy, Er). J Appl Phys 97:10A925(1)–10A925(3). doi:10.1063/1.1855707

Morais EA, Luis Scalvi VA (2007) Decay of photo-excited conductivity of Er-doped SnO_2 thin films. J Mater Sci 42:2216–2221. doi:10.1007/s10853-006-1320-0

Ogale SB, Choudhary RJ, Buban JP, Lofland SE, Shinde SR, Kale SN, Kulkarni VN, Higgins J, Lanci C, Simpson JR, Browning ND, Sarma SD, Drew HD, Greene RL, Venkatesan T (2003) High temperature ferromagnetism with a giant magnetic moment in transparent Co-doped SnO_2. Phys Rev Lett 91:077205(1)–077205(4). doi:10.1103/PhysRevLett.91.077205

Ohno H (1998) Making nonmagnetic semiconductors ferromagnetic. Science 281:951–956. doi:10.1126/science.281.5379.951

Ohno H, Munekata H, Penney T, Von Molnar S, Chang LL (1992) Magnetotransport properties of p-type (In, Mn)As diluted magnetic III-V semiconductors. Phys Rev Lett 68:2664–2667. doi:10.1103/PhysRevLett.68.2664

Ohno H, Shen A, Matsukura F, Oiwa A, Endo A, Katsumoto S, Iye Y (1996) (Ga, Mn)As: a new diluted magnetic semiconductor based on GaAs. Appl Phys Lett 69:363–365. doi:10.1063/1.118061

Paul Joseph D, Venkateswaran C (2010) Room temperature ferromagnetism in Cr doped chalcopyrite type Cu-Zn-Se compound. Phys Status Solidi A 207:2549–2552. doi:10.1002/pssa.201026179

Paul Joseph D, Renugambal P, Saravanan M, Philip Raja S, Venkateswaran C (2009) Effect of Li doping on the structural, optical and electrical properties of spray deposited SnO_2 thin films. Thin Solid Films 517:6129. doi:10.1016/j.tsf.2009.04.047

Reed ML, El-Masry NA, Stadelmaier HH, Ritums MK, Reed MJ, Parker CA, Roberts JC, Bedair SM (2001) Room temperature ferromagnetic properties of (Ga, Mn)N. Appl Phys Lett 79:3473–3475. doi:10.1063/1.1419231

Ruderman MA, Kittel C (1954) Indirect exchange coupling of nuclear magnetic moments by conduction electrons. Phys Rev 96:99–102. doi:10.1103/PhysRev.96.99

Sambasivam S, Choi BC, Lin JG (2011) Intrinsic magnetism in Fe doped SnO_2 nanoparticles. J Solid State Chem 184:199–203. doi:10.1016/j.jssc.2010.11.010

Soumahoro I, Moubah R, Schmerber G, Colis S, Ait Aouaj M, Abd-lefdil M, Hassanain N, Berrada A, Dinia A (2010) Structural, optical, and magnetic properties of Fe-doped ZnO films prepared by spray pyrolysis method. Thin Solid Films 518:4593. doi:10.1016/j.tsf.2009.12.039

Sundaresan A, Bhargavi R, Rangarajan N, Siddesh U, Rao CNR (2006) Ferromagnetism as a universal feature of nanoparticles of the otherwise nonmagnetic oxides. Phys Rev B 74:161306. doi:10.1103/PhysRevB.74.161306

Tarey RD, Raju TA (1985) A method for the deposition of transparent conducting thin films of tin oxide. Thin Solid Films 128:181–189

Ting C-C, Chen S-Y, Hsieh W-F, Lee H-Y (2001) Effects of yttrium codoping on photoluminescence of erbium-doped TiO_2 films. J Appl Phys 90(11):5564–5569. doi:10.1063/1.1413490

Wang D, Wen S, Chen J, Zhang S, Li F (1994) Microstructure of SnO_2. Phys Rev B 49:14282–14285. doi:10.1103/PhysRevB.49.14282

Wang W, Wang Z, Hong Y, Tang J, Yu M (2006) Structure and magnetic properties of Cr/Fe-doped SnO_2 thin films. J Appl Phys 99:08M115. doi:10.1063/1.2171940

Wu J, Coffer JL (2007) Strongly emissive erbium doped tin oxide nanofibers derived from sol gel/electrospinning methods. J Phys Chem C 111:16088–16091. doi:10.1021/jp076338y

Yang S, Evans SM, Halliburton LE, Slack GA, Schujman SB, Morgan KE, Bondokov RT, Mueller SG (2009) Electron paramagnetic resonance of Er^{3+} ions in aluminum nitride. J Appl Phys 105:023714. doi:10.1063/1.3065532

Yosida K (1957) Magnetic properties of Cu-Mn alloys. Phys Rev 106:893–898. doi:10.1103/PhysRev.106.893